Measurements of pore-scale water flow through snow using fluorescent particle velocimetry

WATER RESOURCES RESEARCH, VOL. 49, 1–9, doi:10.1002/2013WR013960, 2013

Measurements of the pore-scale water flow through snow using Fluorescent Particle Tracking Velocimetry

B. Walter,[1] S. Horender,[1] C. Gromke,[2] and M. Lehning[1,3]

Received 12 April 2013; revised 5 October 2013; accepted 7 October 2013.

[1] Fluorescent Particle Tracking Velocimetry (FPTV) measurements of the pore-scale water flow through the pore space of a wet-snow sample are presented to demonstrate the applicability of this measurement technique for snow. For the experiments, ice-cooled water seeded with micron sized fluorescent tracer particles is either sprinkled on top of a snow sample to investigate saturated and unsaturated gravity-driven flow or supplied from a reservoir below the snow sample to generate upward flow driven by capillary forces. The snow sample is illuminated with a laser light sheet and the fluorescent light of the particles transported with the water in the pore space is recorded with a high-speed camera equipped with an optical filter. Tracking algorithms are applied to the images to obtain flow paths and flow velocities. A flow loop found in a pore space for the case of saturated gravity flow together with the tortuosity of the particle trajectories indicate the three-dimensionality of the water flow in wet snow. The average vertical flow velocities in the pore spaces were 11.2 mm s^{-1} for the downward saturated gravity flow and 9.6 mm s^{-1} for the upward flow that is driven by capillary forces for the limited cases presented as examples of the measurement technique. In the case of unsaturated gravity-driven flow, the average and the maximum flow velocities were found to be 30 times smaller than for the saturated gravity flow. Velocity histograms show that the fraction of the total water flowing against the main flow direction was about 3–5%, and that the horizontal velocities average to zero for both the saturated gravity-driven and the capillary flow.

Citation: Walter, B., S. Horender, C. Gromke, and M. Lehning (2013), Measurements of the pore-scale water flow through snow using Fluorescent Particle Tracking Velocimetry, *Water Resour. Res.*, *49*, doi:10.1002/2013WR013960.

1. Introduction and Background

[2] Investigations of the water flow through the pore space of snow are particularly important to understand the formation of wet-snow avalanches or floods due to melt water run off. Both are natural hazards threatening alpine communities and infrastructures such as roads and railways in springtime when snowmelt establishes. A wet snowpack is typically a result of increased solar irradiation, sensible heat fluxes into the snowpack, rain on snow, or melt from below arising from warm soil beneath the snowpack [e.g., *Brooks and Williams*, 1999; *Marsh*, 2006]. For each of these cases, the redistribution of the liquid water within the snowpack is governed by gravitational, viscous, and capillary or surface tension forces [e.g., *Colbeck*, 1972]. Typically two flow types can be distinguished in snow: matrix flow and preferential flow. While the flow is more or less homogenously distributed over the pore space in case of the matrix flow, preferential flow incorporates favorable vertical flow paths consisting of a system of pores that can be up to a few centimeters wide [e.g., *Waldner et al*., 2004; *Williams et al*., 2010]. Within these preferential flow paths, the flow through the pore space can be near saturation [e.g., *Waldner et al*., 2004], whereas for the surrounding matrix flow, the flow is typically unsaturated with a volumetric liquid water content θ_w less than about 0.08 [e.g., *Mitterer et al*., 2011]. However, it remains unclear which processes are responsible for preferential flow path generation [*Waldner et al*., 2004]. Furthermore, phase change processes between ice, water, and water vapor result in snow metamorphism and thus in a change of the pore space of the snow matrix [e.g., *Lehning et al*., 2002; *Daanen and Nieber*, 2009]. Such changes typically have a significant influence on the hydraulic properties such as the water retention capability or the hydraulic conductivity of snow. These properties are essential to accurately describe unsaturated water flow in porous media by means of continuum models like the Richards equation [*Richards*, 1931] and thus to determine the correct timing and magnitude of water flow in snow [*Shimizu*, 1970; *Yamaguchi et al*., 2010; *Hirashima et al*., 2010; *Mitterer et al*., 2011; *Kattelmann and Elder*, 2008; *Wever et al*., 2013].

[3] However, most previous studies mainly quantified the total flow through the snow matrix for different

[1]Unit Snow and Permafrost, WSL Institute for Snow and Avalanche Research SLF, Davos, Switzerland.
[2]Unit Building Physics and Services, Eindhoven University of Technology, Eindhoven, Netherlands.
[3]CRYOS, School of Architecture, Civil and Environmental Engineering, École Polytechnique Fédéral de Lausanne, Lausanne, Switzerland.

Corresponding author: B. Walter, WSL Institute for Snow and Avalanche Research SLF, Flüelastrasse 11, CH-7260 Davos, Switzerland. (walter@slf.ch)

0043-1397/13/10.1002/2013WR013960

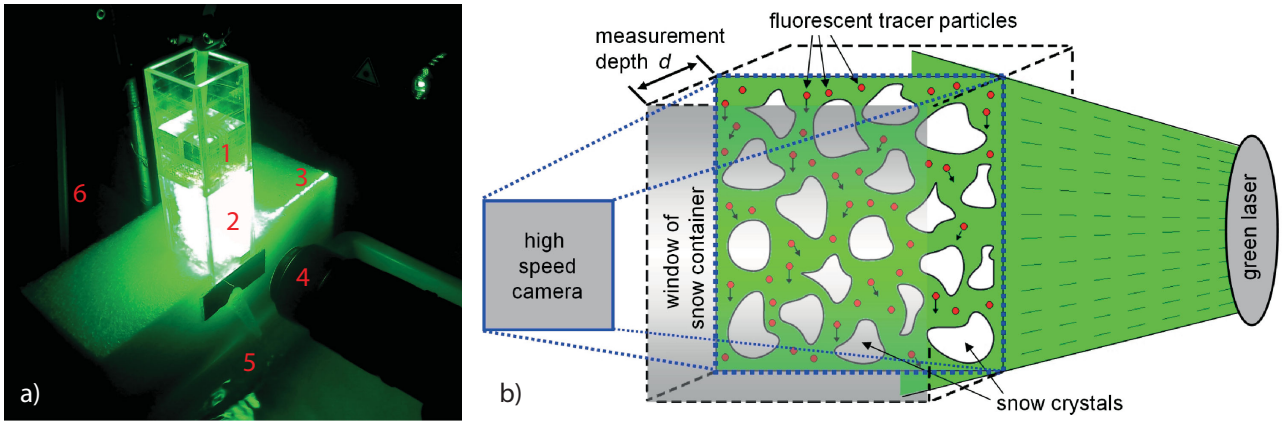

Figure 1. Experimental setup: (a) 1: upper reservoir with seeded water; 2: lower reservoir with wet-snow sample; 3: laser light sheet; 4: lens of high-speed camera with cut-on filter; 5: water basin; and 6: tube for pumping water into upper reservoir. (b) Schematic drawing of the measurement principle which is rotated by 90° clockwise in relation to Figure 1(a).

snowpack layers neglecting dynamics of the pore-scale flow [e.g., *Colbeck*, 1972, 1976; *Colbeck and Anderson*, 1982; *Jordan*, 1983]. A detailed description as a basis for quantitative understanding, however, requires investigations of the microscale flow dynamics and their interaction with related processes that happen at the pore scale, for example, phase changes due to wet-snow metamorphism. Wet-snow metamorphism is a process that changes the snow structure as water percolates through the snow matrix, resulting in an average snow grain growth and subsequent changes in pore sizes and pore size distribution [e.g., *Brun*, 1989; *Lehning et al.*, 2002]. These changes of the pore space further influence the water flow properties including the hydraulic conductivity, flow velocities, and flow paths. New measurement techniques like Fluorescent Particle Tracking Velocimetry (FPTV) can provide spatially and temporally resolved flow measurements to investigate the flow at the pore scale as well as the influence of wet-snow metamorphism on the flow.

[4] In this study, we present spatiotemporally highly resolved Fluorescent Particle Tracking Velocimetry (FPTV) measurements of water flow in the pore space of a wet-snow sample as demonstrative cases to demonstrate a new, powerful measurement technique for gaining deeper insight into the water flow dynamics and related processes in snow. As a first attempt, we present flow results for both a saturated and unsaturated gravity-driven flow as well as for an upward flow, solely driven by capillary forces.

[5] FPTV measurements were extensively used for investigations of the flow fields in porous media and fills [e.g., *Northrup et al.*, 1991; *Arthur et al.*, 2009]; however, to our best knowledge, this is the first study applying FPTV to snow. The presented experiments show that FPTV measurements in snow are feasible and that the results provide useful insight into the water flow dynamics in snow. Such data might, for example, be useful to parameterize new formalisms used to describe the flow in porous media like the Soil Drainage Foam Equation (SDFE) [*Or and Assouline*, 2013], or to validate and test numerical models. It could also generate a deeper understanding of parameters typically used in continuum descriptions of water flow, such as parameterizations of the matrix potential as a function of the liquid water content [e.g., *Yamaguchi et al.*, 2010]. FPTV may open a wide range of investigations of water percolation through a snowpack under various atmospheric and snow conditions. Potential future investigations include analyzing water flow paths and flow velocities in snow, capillary barriers in stratified snow, the transitions from melt water at the snow grain surface to water-filled pores, the transition from water-filled pores to melt water percolation, the redistribution of water at an impermeable layer, and the transport of particles such as algae or particulate matter within the snowpack.

2. Experimental Setup and Measurement Technique

[6] The experimental setup for the gravity-driven, saturated water flow consists of two rectangular acrylic glass reservoirs, each of dimension $50 \times 50 \times 100$ mm^3 stacked on top of each other (Figure 1a). The bottom of the upper reservoir is perforated to carefully sprinkle the ice-cooled water that is seeded with fluorescent tracer particles on top of the wet-snow sample in the lower reservoir. Natural melt form grains were carefully sieved into the sample reservoir for preparing the snow samples. The initial liquid water contents of the snow samples were not determined. When sprinkling the seeded water on top of the wet-snow sample (of density approximately 400 kg/m^3), the water percolates downward through the pore space driven by gravity. The water below the snow sample is collected in a water basin where it is cooled with ice and manually mixed to generate a homogeneous suspension. From there, the water is pumped back into the upper reservoir to be used again. The wet-snow sample is illuminated with a green, about 1 mm wide laser light sheet from the side (Figures 1a and 1b). The laser is a 5 W Diode Pumped Solid State (DPSS) 532 nm cw-laser and the excited fluorescent particles (Rhodamin B doped Polymethylmethacrylat (PMMA), diameter range: 20–50 μm, density: 1.19 g cm^{-1}) emit light at a wavelength of 584 nm. The particle relaxation time of the fluorescent tracers in water is $\tau_p = 3.7 \times 10^{-6}$ s, suggesting

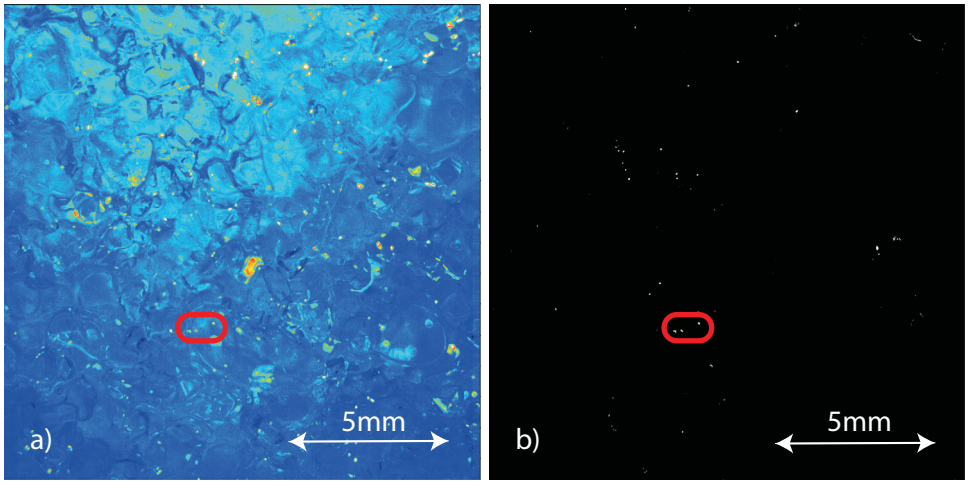

Figure 2. (a) Raw image (false colors) of the high-speed recording where the small bright spots are the fluorescent tracer particles. The wet-snow matrix is indicated by the background image. (b) Processed image used for particle tracking.

an ideal flow following behavior, such that the particle velocities represent the local water flow velocities [*Brenner*, 2012]. The trajectories of the particles are filmed with a high-speed camera (High Speed Star 5.1, LaVision, Complementary Metal Oxide Semiconductor (CMOS) sensor, recording rate: 200 Hz) equipped with a macrolens (Nikon Micro-Nikkor 70–180 mm with 4 cm additional spacing between the chip and the lens) and a high-pass filter with a cut-on frequency of 540 nm.

[7] The seeding density of the fluorescent particles in the water was relatively low about 0.5 mg/L for the experiments presented here. Higher particle densities would be helpful to obtain a better representation and a higher accuracy of the pore-scale water flow in snow in future studies. The maximum measurement resolution with our setup was 15 μm $\times$15 μm per pixel, resulting in a measurement window of about 15 mm $\times$15 mm. The rather large fluorescent particles, compared to the average pore size, which was estimated from the FPTV images being about 0.3 mm, inhibits the determination of near-wall velocities which are missing in the flow analysis presented below. A solution to this problem may be the use of smaller fluorescent particles, which then, however, would require higher image resolutions. We want to re-emphasize that the intention of this study is to present a new tool for investigating water flow at the pore scale in snow, including some first results, which leaves room for improvements and more detailed future studies.

[8] The nonintrusive measurement of velocities in multiphase porous media using optical detection techniques typically requires refractive index matching [e.g., *Northrup et al*., 1991]. This means that the refractive indices of the fluid phase and of the solid phase of the porous medium need to be identical such that the system becomes transparent, thus resulting in direct optical access to the pore space [*Wiederseiner et al*., 2010]. The refractive index n of water at an atmospheric pressure of 1 bar, a temperature of 0°C, and a wavelength of $\lambda = 589$ nm is $n = 1.33346$ [*Thormählen et al*., 1985], while ice has a refractive index of about $n = 1.309$ under similar conditions. Thus, the advantage of our setup over comparable studies typically using acrylic materials with $n \approx 1.49$ [e.g., *Arthur et al*., 2009] is that the refractive indices of water and ice are quite similar. Nevertheless, even a difference of about $\Delta n = n_{\mathrm{water}} - n_{\mathrm{ice}} \approx 0.02$ results in blurry fluorescent particles filmed with the camera once the light passes more than one or two ice-water interfaces in the case of saturated flows. This limits the possible measurement depth of this experimental setup to a focal plane of less than 5 mm behind the acrylic glass of the snow sample reservoir (Figure 1b) for the saturated flow cases. At this depth, the influences of the surface forces of the acrylic glass on the water flow are assumed to be negligibly small as the focal plane was at least one snow grain diameter away from the acrylic glass window. The measurements on saturated flows presented here were recorded with a 1 mm thick focal plane about 4 mm behind the reservoir glass. The size of the wet-snow grains was about 0.5–2 mm. To obtain larger measurement depths, however, refractive index matching is required, which can be achieved by adding liquids to the water with a refractive index lower than that of ice.

[9] For the case of unsaturated flow, refractive index matching is not possible because of the air phase. To avoid the influence of water droplets sticking at the walls of the reservoir for the case of the unsaturated flow presented in section 3.3, the front glass has been removed to obtain direct optical access to the snow matrix. However, owing to the air phase, only the water flow in crevices close to the exposed vertical snow surface was filmed. Figure 2a shows a raw image of a water-saturated wet-snow sample in the lower reservoir (Figure 1a) with small bright spots (e.g., as indicated in the red circle) which are the fluorescent tracer particles. The background image reveals the structure of the snow sample where melt form grains [*IACS*, 2009] with an average diameter of about 1 mm can be identified. However, the background image does not allow for a detailed characterization of the snow sample and the pore space owing to the limited resolution. This would require additional measurement techniques such as computer tomography [e.g., *Coléou et al*., 2001]. Blurry particles in the

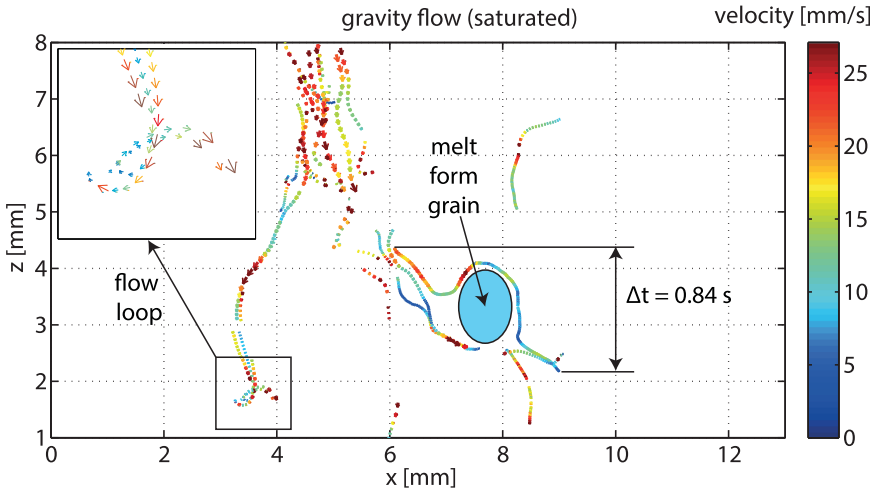

Figure 3. Particle trajectories for the downward saturated gravity-driven flow. Colors of arrows indicate particle velocities. The image shows about 30 individual particle tracks.

image are a result of differences in the refractive indices of water and ice. The few large bright spots in Figure 2a are most likely particles that have become stuck behind snow grains. The particles may either get stuck in small crevices or may sediment due to gravity at locations of very low flow velocities close to or equal to zero; in the latter case, the particles do not represent the local flow velocities and flow paths. The stuck particles result in bright spots which disturb the images. Along with the expense of the particles, the particles getting stuck have been the two main reasons for the rather low seeding density. The raw images are then processed by applying two graphical filters: the subtraction of a constant value and of a sliding average to remove the background, so that only the moving fluorescent particles remain before applying the tracking algorithm (Figure 2b). The algorithm then detects the individual particles in the consecutive images and calculates the corresponding velocity vectors. For the high-speed recording, the image post-processing and the tracer particle tracking, the software Davis (Version 8.10, LaVision (2011), Göttingen) was used.

3. Results and Discussion

3.1. Saturated Gravity Flow Example

[10] The particle trajectories and flow velocities for the case of the saturated gravity flow are shown in Figure 3. Each vector is labeled with a color indicating the particle velocity at specific particle locations. The water supply rate on top of the snow sample was about 1 mm s^{-1} and the total measurement time was 1.35 s. The liquid water content was not measured, however, observing the sample visually clearly suggested a saturated flow condition. The longest particle track had a travel time of $\Delta t = 0.84$ s and the path of this particle shows a strong deflection around a melt form grain, with a diameter of about 1 mm which acts as a barrier within the water flow path. This strong deflection results locally in an upward flow opposite to the average water flow which was downward in the negative z direction. This flow path indicates that the tortuosity of the water flow in the pore space of snow may locally be quite high.

[11] A wider flow path, about 1.5 mm in diameter, with a relatively high particle density and high particle velocities occurred around $\{x, z\} = \{5$ mm, 7 mm$\}$ in Figure 3, suggesting the existence of a favorable flow path (not to be confused with preferential flow paths for unsaturated flows in snow covers that can be up to a few centimeters wide). This flow path is most likely a result of a larger pore space draining most of the water of its surrounding pore spaces. Although the particle velocities are relatively high within that flow path, there are still strong velocity variations between different particles. The variations may either be a result of a not yet stationary flow, although the experiment had already been running for several minutes, or the spatial inhomogeneity of the flow over the flow path cross section as exhibited by the velocity gradient. Strictly speaking, a fully stationary flow will never develop because of wet-snow metamorphism, which results in a continuously changing snow matrix and pore space available for the water flow. Nevertheless, wet-snow metamorphism happens at large time scales compared to the measurement time of a few seconds presented here. Therefore, we attribute the observed velocity variations to the flow inhomogeneity, which results in higher velocities in the middle of the flow path and in lower velocities close to the ice surface of the snow matrix where the nonslip condition [e.g., *Tritton*, 1988] holds (Figure 3). The Reynolds number of this saturated water flow is $\mathrm{Re}_d = Ud/\nu = 5.5$, where $U = 10$ mm s^{-1} is the average velocity in the pore space, $d = 1$ mm the average pore diameter and $\nu = 1.8 \times 10^{-6}$ m^2 s^{-1} is the kinematic viscosity of liquid water at about 0°C. A Reynolds number below $\mathrm{Re} < 10$ indicates a laminar flow without vortex shedding where viscous forces cannot be neglected.

[12] Another interesting feature is observed at $\{x, z\} = \{4$ mm, 2 mm$\}$ in Figure 3. Particles enter a small pore space with a relatively high velocity of about 20–25 mm s^{-1}, and are deflected by the snow matrix, performing an almost 360° loop at a lower velocity around 10–15 mm s^{-1}, and leave the pore space again at a higher velocity. This flow loop suggests the existence of vortex-like

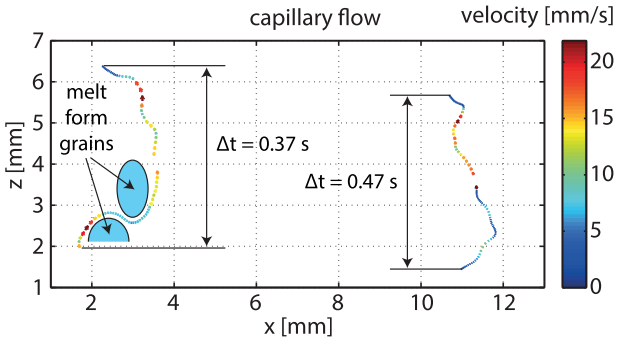

Figure 4. Particle trajectories for the upward flow driven by capillary forces. Colors of arrows indicate particle velocities.

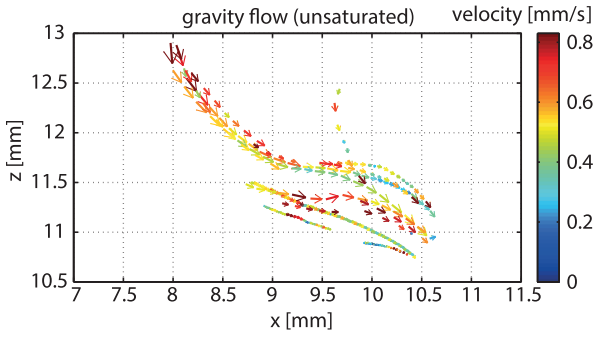

Figure 5. Particle trajectories for the downward unsaturated gravity-driven flow. Colors of arrows indicate particle velocities. The figure represents a zoom into a region of the recorded images where particles were successfully tracked.

flow structures generated by the complex flow system in the pore space of the snow. The flow loop and the other trajectories show that the flow within the snow sample is three-dimensional. This three-dimensionality is one of the two reasons why the fluorescent particles can only be tracked over small distances. Most particles are only in the focal plane, which was only about 1 mm, for a short period of time. The second reason for the limited tracking distances is that the optical access is limited, since no refractive index matching has been performed (see section 2). Once the fluorescent light of the particles has to pass through several ice-water boundaries, the particles become too blurry to be tracked.

3.2. Flow Driven by Capillary Forces: Demonstrative Case

[13] In a second experiment, the snow sample in the lower reservoir (Figure 1a) was carefully placed in a Petri dish filled with seeded, ice-cooled water. Owing to capillary action, the water level was raised up within the snow sample to a height where the gravitational force of the water column equals the capillary forces. The FPTV measurements were performed while the water flowed upward within the pore space of the wet-snow sample.

[14] Figure 4 shows two trajectories of fluorescent particles moving upward due to the flow driven by the capillary action. The seeding particles in the water-filled Petri dish were mixed by hand, but sedimented at around 0.04 mm s^{-1} during the measurement preparation. As a result, the uppermost 0.5–1 mm of the water in the petri dish showed a smaller concentration of tracer particles and thus, only two particles could be observed during the total measurement time of 1.35 s. The travel time of both particles is given in Figure 4. The left particle trajectory also shows a strong deflection of the water around a wet-snow crystal resulting in a short section of about $\Delta z = 0.5$ mm where the vertical flow is negative against the main (upward) flow direction. This also suggests a relatively high tortuosity of the flow paths for the case of the capillary flow. Only tracking two particles is insufficient to draw general conclusions on the capillary flow, however, the results provide useful insight into the flow paths and the flow dynamics as presented in section 3.4.2. Both trajectories end at a height of approximately $z = 6$ mm because the gravitational forces balance the capillary forces on the water and the fluorescent particles do not get transported higher up within the pore space of the snow matrix. This interpretation is well supported by the strongly decreasing velocities at the upper end of the particle trajectories. Owing to the rather simple experimental setup, it was not possible to relate the height of the tracked particles to the height of the water level in the Petri dish, which slightly decreased because of the finite volume of water in the dish. Therefore, it was not possible to estimate the average pore diameter based on the level of rise. However, the lower part of the snow sample was always fully saturated.

3.3. Unsaturated Gravity Flow Example

[15] In this section, we demonstrate the applicability of the FPTV measurement technique for unsaturated flow conditions. The unsaturated water flow through a wet-snow sample was investigated using a slightly modified experimental setup, allowing for a reduced water supply rate on top of the sample with an intensity of about 1 mm min^{-1} (instead of about 1 mm s^{-1} used for the saturated flow case). This was achieved by spraying the water on top of the snow sample using a finer nozzle. The capillary number $Ca = \mu V/\gamma$ was 1×10^{-5} indicating that the flow was dominated by capillary forces. Here, $\mu = 1.8$ mPa s is the dynamic viscosity of water and $\gamma = 75$ mN m^{-1} the interfacial tension between water and air at the melting point. $V = 0.4$ mm s^{-1} is the average flow velocity as will be presented later. The images were recorded at a frequency of 60 Hz. The results reveal strongly reduced velocities compared to the saturated flow case as expected (Figure 5). In this unsaturated flow example, a rather small section of the snow sample of about 5 mm × 5 mm was successfully filmed and evaluated resulting in reasonable particle velocities and trajectories. The results do not represent a generally valid velocity distribution within the pore space; nevertheless, they give a preliminary idea of possible pore-scale flow velocities for an unsaturated case. Most likely, only the flow in one crevice or flow path has been filmed in this case, which is reflected by the fact that all tracked particles show trajectories from the upper left to the lower right (Figure 5). For these reasons, no velocity statistics are presented for the unsaturated flow in the following section.

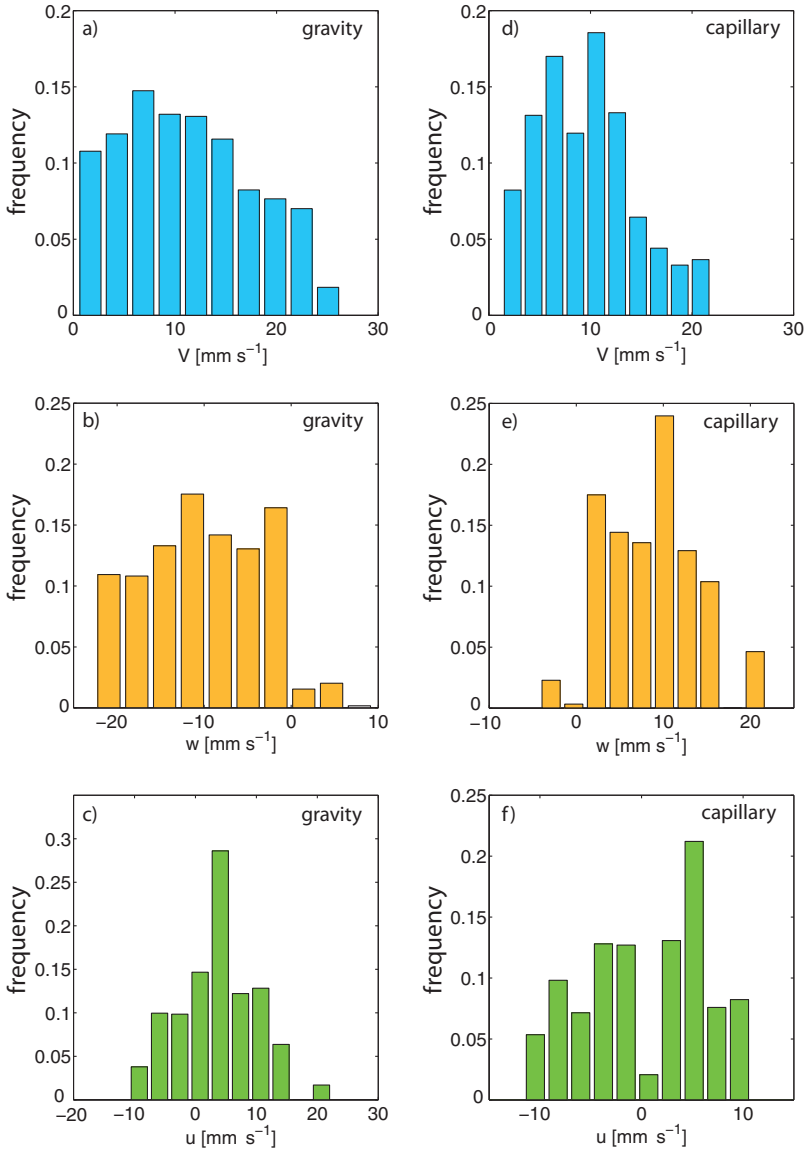

Figure 6. (a–c) Velocity histograms for the saturated gravity flow and (d–f) the capillary flow for the absolute velocities V, the vertical velocities w, and the horizontal velocities u.

Nevertheless, the maximum and the average flow velocities were found to be 0.83 and 0.38 mm s^{-1} (27.1 and 11.2 mm s^{-1} for the saturated flow from Figure 3, respectively). These velocities are about 30 times smaller than the corresponding velocities for the saturated gravity flow. This example shows that FPTV measurements for the case of unsaturated flow are in principle feasible, despite the fact that the air phase results in reflections and refractions disturbing the images. Reflections of about the size of the tracer particles can typically not be tracked over long distances, normally only on a few images, because they strongly change their size and light intensities on the images in time and space. The reflections that may result in erroneous particle tracks and flow results can be removed by defining well-tracked particles as those that are tracked over rather long distances, e.g., at least 20 successive images.

3.4. Velocity Statistics

[16] The following analysis on flow velocity statistics is based on the measured particle trajectories shown in Figures 3 and 4. However, for our demonstrative measurements, the number of tracked particles was too low for claiming that the flow velocity distributions are generally valid.

3.4.1. Gravity Flow

[17] The distribution of the absolute velocities, here defined as $V(x, y, t) = [u^2(x, y, t) + w^2(x, y, t)]^{1/2}$ of all velocity vectors in Figure 3 is shown by the histogram in Figure 6a. Here, w is the vertical and u is the horizontal velocity component. The histogram is scaled with the flow velocity since slow particles result in more velocity vectors than fast particles per unit area and time [*Horender*, 2013; *Petrie et al.*, 1988]. Nonmoving particles that might be found in inactive pores were not tracked and are not contributing to this evaluation. The histogram thus represents

the water flow velocity distribution in the active pore space of the wet-snow sample under the following four assumptions: (i) the particles have an ideal flow following behavior, (ii) the particle velocities adequately represent the average water flow velocity at a specific location within the pore space, (iii) the measurement window and the measured trajectories are representative for the water flow within the entire snow sample, and (iv) the water flow is stationary or the measurement time is long enough to obtain a statistical representation of the flow dynamics.

[18] The first assumption was already discussed in the section 2 and holds for all examples presented here. The second assumption strongly depends on the velocity gradients over the cross section of a specific flow path and the location of the tracer particle within that cross section. For the gravity flow, the wider flow path in Figure 3 shows various particle velocities at different locations within the flow path, either because of velocity gradients or a nonstationary flow, so the larger number of tracked particles there are assumed to sufficiently represent the flow within that path. Fewer particles tracked in smaller flow paths might generate larger errors; however, the contribution of those narrow flow paths to the total flow or the total pore space is correspondingly smaller. The measurement window (assumption iii) is assumed to be sufficiently large (7 mm $\times$ 13 mm for the gravity flow), containing about 100 wet-snow grains, which should provide a statistically representative picture for the entire snow sample. However, for our demonstrative measurements (Figures 3–5), the seeding density and thus the number of tracked particles was too low for claiming that the flow velocity distributions are generally valid. For the unsaturated flow (Figure 5), the measurement window was smaller, thus the results do not statistically represent the general flow in the pore space. The measurement time of 1.35 s (assumption iv), limited by our FPTV setup, is too short if the state of being stationary is only assumed and not guaranteed. Despite the above discussed assumptions and limitations, the velocity statistics as presented in this section provide useful insight into the water flow dynamics in the pore space of snow.

[19] The scaled histogram for the absolute velocities (Figure 6a) suggests a lognormal or gamma distribution; however, there is no significant decrease in the distribution toward low flow velocities, as it should be for those distributions. Using small tracer particles (<4 μm) together with a larger seeding density would allow for resolving the low flow velocities in the smaller pores. We would expect a widening of the distributions for this case. The occurrence of the many low flow velocities close to zero for the gravity flow may be a result of tracer particles that get trapped in inactive pore spaces, where the water flow is zero or close to zero, and that do not contribute to the overall water drainage. This is only true for a flow close to the state of being stationary where all flow paths are fully developed. In the following section, we show that such low flow velocities do not occur for the nonstationary capillary flow, where the particles get transported within the nonequilibrium flow of the wetting front. The average particle velocity for the gravity flow determined from the scaled velocity histogram (Figure 6a) was $V_{\mathrm{avg}} = 11.2$ mm s^{-1}. The maximum velocity was $V_{\mathrm{max}} = 27.1$ mm s^{-1}. Figure 6b shows the scaled histogram for the vertical velocities $w(x, y, t)$ of all tracked particles from Figure 3, representing the vertical flow in the pore space. It shows that in about 5% of the pore space, the flow was directed upward (positive w-values) against the main flow direction, which was downward for the gravity flow. The negative w-velocities are more or less homogenously distributed over the entire velocity range from -20 to 0 mm s^{-1}, with an average value of $w_{\mathrm{avg}} = -10.1$ mm s^{-1}. This value agrees very well with velocities found in preferential flow paths where the flow can locally be near saturation [*Waldner et al*., 2004], suggesting that the flow dynamics for the saturated gravity flow presented here approximate the flow in preferential flow paths.

[20] The maximum vertical and horizontal particle velocities were -22.5 and $+22.4$ mm s^{-1}, respectively. Figure 6c shows the scaled histogram for the horizontal u-velocities which is centered at about zero because there is no net flow in x-direction and the sample is assumed to be homogenous. The distribution not being exactly centered at zero is a result of the limited measurement window and the relatively low seeding density as discussed above, giving an idea of how well the measurements statistically represent the flow. For an ideal representation of the water flow within the pore space of snow, these u-velocities should be normally distributed and perfectly centered at zero. A normal distribution is suggested owing to the statistics of the process of flow deflection around snow grains, resulting in both positive or negative u-velocities, and the velocity profiles within the pores. Generally, no distribution fitting has been attempted in this work because of the limited amount of data available. The velocity vectors from the particle trajectories in Figure 3 also allowed for determining flow accelerations and decelerations. The maximum flow acceleration was $+2.1$ m s^{-2} and the maximum flow deceleration was -1.5 m s^{-2} for the gravity-driven flow.

3.4.2. Capillary Flow

[21] The distribution of the $V(x, y, t)$ particle velocities for the capillary flow from Figure 4 is shown by the histogram in Figure 6d. The average flow velocity was $V_{\mathrm{avg}} = 9.6$ mm s^{-1}, which is only slightly lower than that for the gravity flow, which was $V_{\mathrm{avg}} = 11.2$ mm s^{-1}. The maximum flow velocity was $V_{\mathrm{max}} = 21.9$ mm s^{-1}, which is also lower than that for the gravity flow ($V_{\mathrm{max}} = 27.1$ mm s^{-1}). One reason for the lower flow velocities is that gravity acts against the mean flow direction. Another reason might be the fact that no favorable wider flow paths with high flow velocities have been developed for the capillary flow like they did for the saturated gravity flow as shown in Figure 3. On the contrary, the capillary suction in the wider flow paths of the upward capillary flow is smaller than in narrower flow paths, so the larger pores are mainly filled rather slowly owing to the larger capillary pressure of the smaller pores.

[22] The histogram for the absolute velocities (Figure 6d) suggests again a lognormal or a gamma distribution with a slight positive skewness; however, the very limited data available from only two tracked particles results in a larger scatter compared to the V-histogram for the gravity-driven flow (Figure 6a). Furthermore, the distribution strongly decreases toward $V = 0$ in contrast to the gravity flow. This suggests that for the typically nonstationary capillary flow, no inactive pore spaces with water at rest exist,

since all interconnected pore spaces become filled during the capillary rise of the water within the wetting front. This finding is also supported by the histograms for the vertical and the horizontal velocities (Figures 6e and 6f), both showing very few particles with velocities close to zero in contrast to the gravity flow (Figures 6b and 6c). The average vertical velocity was $w_{avg} = +8.6$ mm s^{-1}, suggesting that the pore space of a snow sample is almost filled as fast by capillary forces as water is drained owing to gravity. The maximum vertical and horizontal flow velocities were $+21.9$ and -11.6 mm s^{-1}. The maximum resolved flow acceleration was $+1.2$ m s^{-2} and the maximum flow deceleration was -1.9 m s^{-2}.

4. Conclusions and Outlook

[23] The presented results show that FPTV measurements of water percolation through snow are in principle feasible in enabling a wide range of possible future investigations that may incorporate analyzing the flow across capillary barriers, the generation of preferential flow paths, or the transport of particles within a snowpack, for example. It was shown that the FPTV measurements can be used to determine velocity statistics that support the improvement of modeling water flow through snow. Such data can then be used to parameterize and validate new models of unsaturated water flow in porous media, for example, the Soil Drainage Foam Equation (SDFE) [*Or* and *Assouline*, 2013]. The geometrically explicit formulation of this theory, based on the description of Poiseuille flow in microscopic flow paths enclosed by snow grains and air, avoids the necessity to parameterize the problematic hydraulic conductivity as indispensable for the Richards equation. Since natural snowpacks are typically layered with strong variations in the hydraulic flow resistance across textural contrasts (capillary barriers), the interpolation of the hydraulic conductivity across these barriers often results in inaccurate descriptions of water fluxes at these interfaces. Here, new geometrically more explicit formalisms of the water flow might be useful for improving the description of the flow across these barriers. In this context, FPTV will provide the relevant information on the flow velocities and flow paths before, directly at, and after those barriers. If and how water flows through or gets laterally redistributed at such interfaces is important information, because wet-snow layers within the snowpack promote the formation of wet-snow avalanches. Future FPTV investigations will, on the one hand, significantly increase the basic knowledge of water flow in snow and, on the other hand, they will lay the foundation for alternative formalisms describing the water flow in snow.

[24] Despite the fact that no refractive index matching (see section 2) has been performed, the water flow within the snowpack was measurable up to a depth of about 3–5 mm behind the acrylic glass of the reservoir for the saturated gravity and capillary flow. Nevertheless, refractive index matching is recommended for future experiments on saturated water flow to improve the optical access to the pore space and the measurement depth, thus avoiding possible influences of the reservoir walls on the water flow. However, under natural conditions, the pore space in the snowpack is typically not saturated with water. It was shown that FPTV also allows for investigating unsaturated flows in snow, where flow velocities about 30 times smaller were found for the unsaturated gravity flow case compared to the saturated case.

[25] Furthermore, the measurement resolution of our setup can be improved down to about 4 μm $\times$ 4 μm using better optics for the high-speed camera together with fluorescent polystyrene particles (1.05 g cm^{-3}) of a size of 5 μm or less. Such a setup needs to be tested and may then even allow for resolving the velocity fields in single pore spaces, and thus investigating processes at the pore scale such as wet-snow metamorphism or the impact of rain droplets on the snow surface.

[26] **Acknowledgments.** We would like to thank the Swiss National Science Foundation (SNF) for financing the Laser Imaging measurement technique (R'Equip grant 206021_133786). Thanks also to the SLF workshop for supporting us with the development and the production of the experimental setup.

References

Arthur, J. K., D. W. Ruth, and M. F. Tachie (2009), PIV measurements of flow through a model porous medium with varying boundary conditions, *J. Fluid Mech.*, *629*, 343–374.

Brenner, H. (2012), Fluid mechanics in fluids at rest, *Phys. Rev. E*, *86*(1), 016307.

Brooks, P. D., and M. W. Williams (1999), Snowpack controls on nitrogen cycling and export in seasonally snow-covered catchments, *Hydrol. Processes*, *13*, 2177–2190.

Brun, E. (1989), Investigation on wet-snow metamorphism in respect of liquid-water content, *Ann. Glaciol.*, *13*, 22–26.

Colbeck, S. C. (1972), Theory of water percolation in snow, *J. Glaciol.*, *11*(63), 369–384.

Colbeck, S. C. (1976), An analysis of water flow in dry snow, *Water Resour. Res.*, *12*(3), 523–527.

Colbeck, S. C., and E. A. Anderson (1982), The permeability of a melting snow cover, *Water Resour. Res.*, *18*(4), 904–908.

Coléou, C., B. Lesaffre, J.-B. Brzoska, W. Ludwig, and E. Boller (2001), Three-dimensional snow images by X-ray microtomography, *Ann. Glaciol.*, *32*, 75–81.

Daanen, R. P., and J. L. Nieber (2009), Model for coupled liquid water flow and heat transport with phase change in a snowpack, *J. Cold Reg. Eng.*, *23*, 43–68.

Hirashima, H., S. Yamaguchi, A. Sato, and M. Lehning (2010), Numerical modeling of liquid water movement through layered snow based on new measurements of the water retention curve, *Cold Reg. Sci. Technol.*, *64*(2), 94–103.

Horender, S. (2013), Turbulent flow downstream of a large solidity perforated plate: Near-field characteristics of interacting jets, *Fluid Dyn. Res.*, *45*, 025501.

IACS (2009), The international classification for seasonal snow on the ground, in *Technical Documents in Hydrology N° 83*, Int. Hydrol. Programme. p 90.

Jordan, P. (1983), Melt water movement in a deep snowpack: 2. Simulation model, *Water Resour. Res.*, *19*(4), 979–985.

Kattelmann, R., and K. Elder (2008), Hydrologic characteristics and water balance of an Alpine Basin in the Sierra Nevada, *Water Resour. Res.*, *27*, 1553–1562, doi:10.1029/90WR02771.

LaVision, (2011), Product-Manual High-Speed-Star 5 and Product-Manual Imaging Tools, Göttingen.

Lehning, M., P. Bartelt, B. Brown, C. Fierz, and P. Satyawali (2002), A physical SNOWPACK model for the Swiss avalanche warning, PART II. Snow microstructure, *Cold Reg. Sci.Technol.*, *35*, 147–167.

Marsh, P. (2006), Water flow through snow and firn, in *Encyclopedia of Hydrological Sciences*, doi:10.1002/0470848944.hsa167.

Mitterer, C., H. Hirashima, and J. Schweizer (2011), Wet-snow instabilities: Comparison of measured and modelled liquid water content and snow stratigraphy, *Ann. Glaciol.*, *52*(58), 201–208.

Northrup, M. A., T. J. Kulp, and S. M. Angel (1991), Fluorescent particle image velocimetry: Application to flow measurement in refractive index-matched porous media, *J. Appl. Opt.*, *30*(21), 3034–3040.

Or, D., and S. Assouline (2013), The foam drainage equation for unsaturated flow in porous media, *Water Resour. Res.*, *49*, doi:10.1002/wrcr.20525.

Petrie, H. L., M. Samimy, and A. L. Addy (1988), Laser Doppler velocity bias in separated turbulent flows, *Exp. Fluids*, *6*(2), 80–88.

Richards, L. A. (1931), Capillary conduction of liquids through porous mediums, *Physics*, *1*(5), 318–333.

Shimizu, H. (1970), Air permeability of deposited snow, *Contrib. Inst. Low Temp. Sci.*, *A22*, 1–32.

Thormählen, I., J. Straub, and U. Grigull (1985), Refractive index of water and its dependence on wavelength, temperature, and density, *J. Phys. Chem. Ref. Data*, *14*(4), 933–945.

Tritton, D. J. (1988), *Physical Fluid Dynamics*, Clarendon, Oxford, U. K.

Waldner, P. A., M. Schneebeli, U. Schultze-Zimmermann, and H. Flühler (2004), Effect of snow structure on water flow and solute transport, *Hydrol. Processes*, *18*, 1271–1290.

Wever, N., C. Fierz, C. Mitterer, H. Hirashima, and M. Lehning (2013), Solving Richards equation for snow improves snowpack meltwater runoff estimations, *Cryosphere Discuss.*, *7*, 2373–2412.

Wiederseiner, S., N. Andreini, G. Epely-Chauvin, and C. Ancey (2010), Refractive-index and density matching in concentrated particle suspensions: A review, *Exp. Fluids*, *50*, 1183–1206.

Williams, M. W., T. A. Erickson, and J. L. Petrzelka (2010), Visualizing meltwater flow through snow at the centimetre-to-metre scale using a snow guillotine, *Hydrol. Processes*, *24*, 2098–2110, doi:10.1002/hyp.7630.

Yamaguchi, S., T. Katsushima, A. Sato, and T. Kumakura (2010), Water retention curve of snow with different grain sizes, *Cold Reg. Sci. Technol.*, *64*, 87–93.